Journal of Applied Polymer Science

Flame retarding mechanism of Polyamide 6 with phosphorus-nitrogen flame retardant and DOPO derivatives

Maolin Li,[1] Yuhua Zhong,[1] Zheng Wang,[1] Andreas Fischer,[2] Florian Ranft,[2] Dietmar Drummer,[2] Wei Wu[1]

[1]Sino-German Joint Research Center of Advanced Materials, School of Materials and Engineering, East China University of Science and Technology, Shanghai 200237, People's Republic of China

[2]Friedrich-Alexander-Universität Erlangen-Nürnberg (FAU), Institute of Polymer Technology, Erlangen, Germany

Correspondence to: D. Drummer (E-mail: drummer@lkt.uni-erlangen.de) and W. Wu (E-mail: wuwei@ecust.edu.cn)

ABSTRACT: A novel flame-retardant composite was prepared by introducing a phosphorus-nitrogen flame retardant and DOPO-SiO_2 into PA6. DOPO-SiO_2 was synthesized successfully in a one-step process. PA6/OP1314/DOPO-SiO_2 achieved a UL 94 V-0 rating with an LOI value of 31%. The maximum mass loss rate of decomposition decreased significantly and char residue increased to 11.6 wt % compared with that of pure PA6. The compacted and dense char was formed due to the combination of the P-N flame retardant and DOPO-SiO_2. The complex viscosity of PA6/OP1314/DOPO-SiO_2 increased considerably which tend to prevent the dripping phenomenon. The flame-retardant mechanism of PA6/OP1314/DOPO-SiO_2 was also investigated by Fourier transform infrared spectroscopy FTIR at different temperatures and the pyrolysis products were investigated by pyrolysis gas chromatography/ mass spectrum (Py-GC/MS). It was assumed that DOPO-SiO_2 and the hypophosphite of OP1314 possess excellent flame retardancy during the gaseous phase. Meanwhile, melamine and phosphate reacted with the pyrolytic products of PA6 to protect the matrix during the condensed phase. © 2015 Wiley Periodicals, Inc. J. Appl. Polym. Sci. **2016**, *133*, 42932.

KEYWORDS: polyamides; spectroscopy; thermogravimetric analysis (TGA)

Received 14 July 2015; accepted 13 September 2015

DOI: 10.1002/app.42932

INTRODUCTION

Polyamide 6 (PA6) is an important engineering plastic with an excellent mechanical strength, high abrasion, self-lubrication, outstanding electric performance, and good processability. PA6 is widely used in the fields of transportation, electrical and electronic applications, telecommunications, chemical and medical engineering. Facing safety regulations, especially in transportation, industry and electronics the flammability of PA6 must be considered. Thus it is imperative to enhance PA6's resistance to flammability.

Exolit OP 1314 is a non-melting salt that contains P-N, is nontoxic, free of heavy metals, environmentally friendly and known to deter flammability in polyamides. The principal component of OP1314 is hypophosphite and melamine polyphosphate, acting as a phosphorus-nitrogen flame retardant. Phosphorus-nitrogen flame retardants have been applied in many different matrices to improve the flame retardancy of polymers. Zhong *et al.*[1] researched the properties and mechanism of thermoplastic poly(ether-ester) elastomer (TPEE) containing aluminum diethyl phosphinate, melamine polyphosphate, and novolac, proving that a P–N flame retardant could significantly improve the limiting oxygen index (LOI) value of TPEE. Bourbigot *et al.*[2] showed that the approach of using "nanocomposites" provides good results combined with conventional flame retardants (phosphinate and phosphate) and leads to synergistic effects[2]. However, simply introducing P-N as a flame retardant cannot prepare samples without melt dripping behavior. In order to achieve PA6's high degree of flame retardancy, DOPO-SiO_2 was introduced into the P-N flame retarding PA6.

Derivatives based on 9,10-dihydro-9-oxa-10-phosphaphenanthrene-10-oxide (DOPO) are an attractive alternative flame retardant for PA6.[3,4] Derivatives based on DOPO were proven effective for bismaleimide resins,[5] epoxy acrylates,[6] polyurethane foams,[7,8] and epoxy resins.[9–12] DOPO and its derivatives are known to predominantly act by a gas-phase mechanism through the formation of PO· radicals. Derivatives based on DOPO are halogen-free and an attractive alternative solution. However, the thermal stability of DOPO has a poor thermal stability. Fumed silica can improve the mechanical properties[13,14] and thermal stability of polymers.[15,16] Nano-silicon dioxide (SiO_2) is a kind of inorganic filler with good a physical barrier effect in the combustion process. However, the agglomeration phenomenon and wick effect of nanoparticles did not disappear in the composites. The most decisive

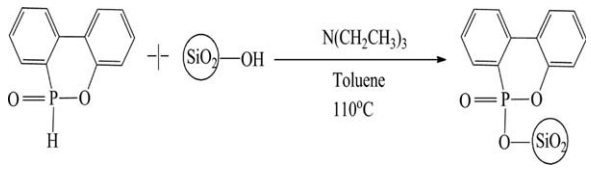

Scheme 1. Preparation of DOPO–SiO_2.

factor when attempting to achieve excellent flame retardant performance is to attain uniform dispersion of the filler particles. Thus, the modifying SiO_2 with DOPO is quite conceivable.

In this paper, we immobilized DOPO on SiO_2 to improve the compatibility and flame retardancy in the matrix. The flame-retarding PA6 composites were prepared through a melt-mixing process. The flammability, thermal stability, char morphology, and rheological properties were examined using the UL94 test, the LOI test, TGA, SEM-EDX, Rotational Rheometry, FTIR and pyrolysis GC/MS. The flame retardant (FR) mechanism of PA6/OP1314/DOPO-SiO_2 was presented through the analysis of the flame retarding action in the gaseous phase and condensed phase.

EXPERIMENTAL

Materials

PA6 pellets (YH-800, melting temperature = 215–220°C, ρ = 1.156 g/cm^3) were purchased from Hunan Yueyang Baling Petrochemical Co., Ltd. (China). Exolit OP 1314 was obtained from Clariant (Germany). DOPO was obtained from Eutec Trading (Shanghai) Co., Ltd. (China). Aerosil-200 fumed SiO_2 (hydrophilic, specific surface area = 200 m^2/g, average particle size = 12 nm, purity = 99.8%, moisture < 1.5%) was purchased from Aladdin.

One-Step Preparation of DOPO–SiO_2

Due to the activity of the P—H bond in DOPO and free silanols on the surface of SiO_2, DOPO and SiO_2—OH directly reacted under the initiation of triethylamine. The reaction was carried out under reflux with a suspension of 5 g of SiO_2—OH nanoparticles and 2 g of DOPO in 200 mL of toluene; we added the components dropwise into the suspension and stirred it continuously under a nitrogen atmosphere for 24 h at 110°C (Scheme 1). Then, the product was filtered and washed with toluene three times until no white solid dissolved out. DOPO–SiO_2 was dried in a vacuum oven for 24 h at 110°C.

Preparation of the PA6 composites

Neat PA6 and the SiO_2 nanoparticles were dried in an oven at 110°C for 8 h, while DOPO and DOPO–SiO_2 were dried at 80°C for 4 h before melt processing. All formulations were melted in a twin-roll mill at 230°C for 8 min at a screw speed of 80 rpm. All are presented in Table I. The size and thickness of all specimens were made suitable for compression molding under constant parameters.

Characterization

Fire Testing. All samples were measured in a vertical burning test (UL 94), for which the dimensions of the specimen were 130 mm × 13 mm × 1.6 mm. The limiting oxygen index (LOI) value was measured according to GB/T2406.2-2009.

FTIR Analysis of DOPO–SiO_2. FTIR spectrometry was performed on KBr pellets with a Thermo Nicolet 6700 FTIR spectrum analyzer in the wave-number range 4000–400 cm^{-1}.

Thermal Analysis. TG measurement was performed on Netzsch STA 409 PC/PG TG analyzer with a nitrogen flow of 40 mL/min. Different samples (5–10 mg) were heated from 30°C to 700°C at heating rates of 15°C/min. The theoretical residue [$W_{(th)}$] was calculated on the basis of the following formula:

$$W_{(th)} = x_1 W_{(ex1)} + x_2 W_{(ex2)} + x_3 W_{(ex3)} + x_4 W_{(ex4)}$$

$$x_1 + x_2 + x_3 + x_4 = 1$$

where $W_{(ex)}$ represents the experimental residue of an individual component and x corresponds to the percentage of mass content in the formulation.

Residues Analysis. A scanning electron microscope (S-4800, Hitachi, Japan) coupled with an X-ray EDS instrument was used to investigate the morphology of the samples. All of the samples were prepared after they were heated at 800°C for 15 min.

Mechanism Analysis. A Thermo Nicolet 6700 FTIR spectrum analyzer was used to test the samples at different temperatures for 15 min.

Py–GC/MS was performed in a Pyroprobe (CDS5000) instrument. The Py chamber was full of He, and the relevant samples (500 μg) were heated from ambient temperature to 600°C. The pyrolyzer was coupled with a GC/MS operation (Agilent 6890/5073). To obtain the gas chromatogram, a metal capillary separation column coated with an immobilized hexamethyl cyclotrisiloxane was heated from 20°C to 270°C at a heating rate of

Table I. Compositions of the Formulations

	Material	PA6 (wt %)	OP1314 (wt %)	DOPO (wt %)	SiO_2 (wt %)	DOPO-SiO_2 (wt %)
S1	PA6	100	—	—	—	—
S2	PA6/OP1314	85	15			—
S3	PA6/OP1314/DOPO	80	15	5	—	—
S4	PA6/OP1314/SiO_2	80	15	—	5	—
S5	PA6/OP1314/DOPO + SiO_2	80	15	0.75	4.25	
S6	PA6/OP1314/DOPO-SiO_2	80	15			5

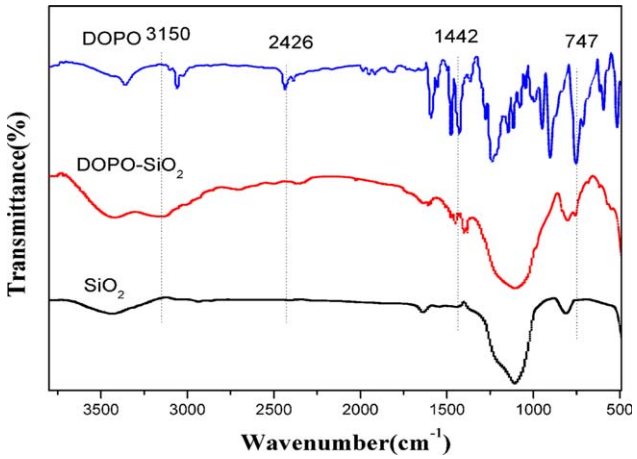

Figure 1. FTIR spectra for DOPO, SiO_2, and DOPO–SiO_2. [Color figure can be viewed in the online issue, which is available at wileyonlinelibrary.com.]

10°C/min and held for 1 min. The detection of mass spectra was carried out with a National Institute of Standards and Technology (NIST) library.

Viscoelastic Analysis. Rheological measurement was performed on a rotational rheometer (MAR3, Haake) with a strain of 1% in a frequency sweep from 0.01 to 100 rad/s at a temperature of 230°C. Samples used for rheological experiments were disks with a diameter of 20 mm and a thickness of 1 mm.

RESULTS AND DISCUSSION

FTIR Analysis of DOPO–SiO_2

The FTIR spectra of SiO_2 and DOPO–SiO_2 are presented in Figure 1. For neat-SiO_2 nanoparticles, two characteristic peaks were around 3200–3650 cm^{-1} (OH stretching vibrations of silanol hydroxyls) and 1000–1100 cm^{-1} (Si—O—Si characteristic vibrations). When DOPO was immobilized on SiO_2, some characteristic peaks of DOPO were observed, The peak at 3150 cm^{-1} was ascribed to the Ar—H stretching vibration, while the peaks at 1442 cm^{-1} and 747 cm^{-1} were assumed to P—Ph and P—O characteristic vibration respectively. The —OH group on the surface of SiO_2 reacted with DOPO resulted in the disappearance of the characteristic peak at 2426 cm^{-1} (P—H DOPO). There is not any other active group can react with the P—H group during the synthesis process. Therefore, DOPO–SiO_2 was synthesized successfully in a one-step process.

Fire Testing

The results of the vertical burning test (UL 94) and the LOI values were presented in Table II. In the UL 94 test, neat PA6 samples were evaluated without a rating, but exhibiting heavy dripping after the first ignition. It is known that samples dripping can cause a great deal of heat to dissipate and prevent further combustion. Comparing PA6/OP1314(S2) with neat PA6(S1), it is clear that the P-N flame retardant effectively enhances the flame retardancy of PA6. The recorded afterflame time of PA6/OP1314 for the first (t_1) and the second (t_2) flame application were 2 s and 8 s. The total afterflame times was 45 s which meets the requirements of UL 94 V-0 rating. Due to melt dripping of S2 after the second ignition, it was rated UL 94 V-2 flammability rating.

With the addition of DOPO, the flammability rating remained at UL94 V-1. Although PA6/OP1314/DOPO(S3) exstinguished at the moment of removing the flame in the first ignition, the second afterflame time was 11 s. This can attribute to the promotion of degradation for the introduction of DOPO. When the nano SiO_2 was added into PA6/OP1314, the dripping phenomenon vanished and the sample attained the UL-94 V-1 rating. The afterflame time increased to a value twice as high as that of PA6/OP1314. As is commonly known, dropping melt dissipates heat and extinguishes flames. Thus, the addition of SiO_2 protects the matrix from burning, eliminating the dripping phenomenon. So, it would extend the time of burning in the second ignition. In order to attain a better flame retardancy, DOPO–SiO_2 was synthesized and introduced to PA6/OP1314. The mixture of the DOPO and SiO_2 was also investigated. The test results of PA6/OP1314/DOPO+SiO_2(S5) were better than that of S3 and PA6/OP1314/SiO_2(S4), which led to the speculation that the combination of DOPO and SiO_2 can enhance the flame retardancy performance. The best result of vertical burning test was PA6/OP1314/DOPO–SiO_2 (S6), achieved the UL-94 V-0 rating. The result was attributed to the flame retarding action of DOPO–SiO_2 in the gaseous phase and condensed phase, it would be discussed in the following section.

The LOI values showed strong correlation with flame retarding mechanism during the gaseous phase[17] and the viscosity of the composite.[18] The LOI value of pristine PA6 was 22.5%. Uploading OP1314, which contained aluminum diethyl phosphinate which had been proven[17] that it could produce phosphorus-containing free radicals that act as radical scavengers to react with active H· and OH· and extinguish fire. The LOI value of S2 increased to 28%. S3 reached a higher LOI value than S2 with DOPO. The LOI value of S4 did no differ from S2. In general, the LOI value of S4 should be higher than that of S2 for the physical barrier of SiO_2. However, the addition of nano-SiO_2 presumably increased the viscosity of the composite and decreased the melt flowability, which negatively affects the LOI value. It was calculated that the SiO_2 merely acts as an inorganic filler. The LOI value of S5 was the same as S3. According to the result from UL-94 vertical burning test, S6 also had the

Table II. Flame Retardancy of the Samples

	UL-94 (1.6 mm)				
Sample	Ranking	t_1/t_2 (s)[a]	$t_1 + t_2$ (s)[b]	Dripping[c]	LOI (%)
S1	No rating	6/—	—	N/Y	22 ± 0.5
S2	V-2	2/8	45	N/Y	28 ± 0.5
S3	V-1	0/11	54	N/N[d]	29 ± 0.5
S4	V-1	4/19	117	N/N	28 ± 0.5
S5	V-1	2/14	60	N/N	29 ± 0.5
S6	V-0	0/4	23	N/N	32 ± 0.5

[a] t_1 or t_2, afterflame times for each individual specimen the first the second ignition.
[b] t_1 and t_2, total afterflame times for two ignitions for the five specimens.
[c] N/Y corresponds to the dripping phenomenon of the first and second ignition.
[d] N/N corresponds to the no dripping phenomenon of the first and second ignition.

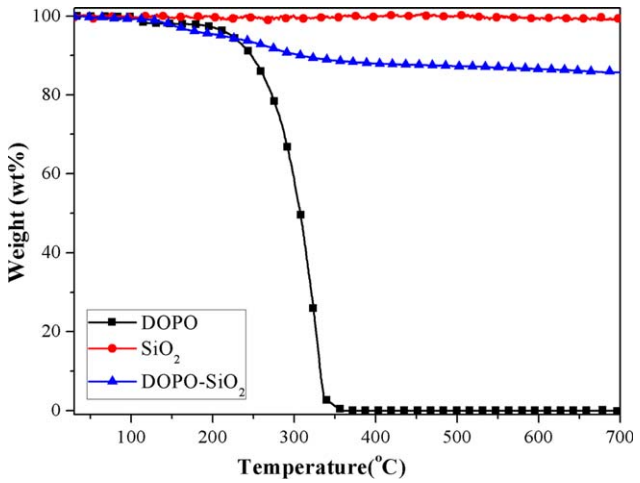

Figure 2. TGA curves for DOPO, SiO_2, and DOPO–SiO_2. [Color figure can be viewed in the online issue, which is available at wileyonlinelibrary.com.]

highest LOI value of 32%. The reason for this will be discussed in the following.

Thermal Analysis

As shown in Figure 2, the initial degradation temperature of DOPO was at 223°C, and the residue close to 0 wt % at 360°C. SiO_2 showed no changes during the heating process. The curve of SiO_2 was a linear. When DOPO was used to modify the SiO_2, the residue of DOPO–SiO_2 was almost 85 wt % at 800°C. The thermogravimetric curve of DOPO–SiO_2 also proved that the DOPO had succeeded in becoming immobilized on SiO_2 corresponding with the result of the FTIR test from the side.

Table III depicts the TG experimental and theoretical results of all the formulations in nitrogen atmosphere. As shown in Fig. 3(a), pure PA6 decomposed in one step, the initial degradation temperature ($T_{5wt\ \%}$) was at 457.1°C and the temperature of maximum mass loss rate (T_{max}) was at 518.9°C, respectively. The main weight loss of S1 in the range 400–500°C resulted

Table III. Thermal Decomposition Data of all Formulation in Nitrogen Atmosphere

Sample	$T_{5wt\ \%}$ (°C)	T_{max} (°C)	Char yield [wt %]	Theoretical char yield [wt %]
S1	457.1	518.9	0.3	0.3
S2	397.5	444.2	4.1	3.4
S3	352.5	419.7	4.8	3.6
S4	360.9	464.4	10.7	8.6
S5	361.5	446.4	9.7	7.2
S6	364.8	464.7	12.0	7.2

from the release of water, carbon monoxide, carbon dioxide, hydronitrogens, and hydrocarbon fragments.[19,20] The char yield at 700°C was 0.3 wt %. The introduction of 15 wt % OP1314 in PA6 enhanced the thermal stability, and the remaining residue was approximately 4.1 wt % at 700°C. Meanwhile, as presented in Figure 3(b), the introduction of OP 1314 decreased the maximum mass loss rate considerably. Compared with PA6, OP1314 decomposed at a lower temperature for the release of the phosphoric acid, which catalyzed the decomposition of PA6 and formed a relatively stable intermediate product that resulted to the decrease of the maximum mass loss rate at high temperature. With the incorporation of DOPO into PA6/OP1314, the initial thermal decomposition temperature decreased, and the rate of maximum mass loss rate increased significantly; the residue increased to 4.9 wt %, which proves that the DOPO can accelerate the decomposition of PA6 and the char-forming process. When SiO_2 was added, $T_{5wt\ \%}$ was at 360.9°C; this value was lower than that of the PA6/OP1314 composite. However, the introduction of SiO_2 significantly decreased the mass loss rate. The improvement of the thermal stability of PA6/OP1314/SiO_2 mainly resulted from the nanoparticles accumulating in the composites; which restricted the movement of the polymer chains, thus resulting in incomplete terminal relaxation.[19] SiO_2 can also form physical barriers to insulate the heat and mass transfer into the underlying polymeric matrix. When DOPO + SiO_2 (2:5) and

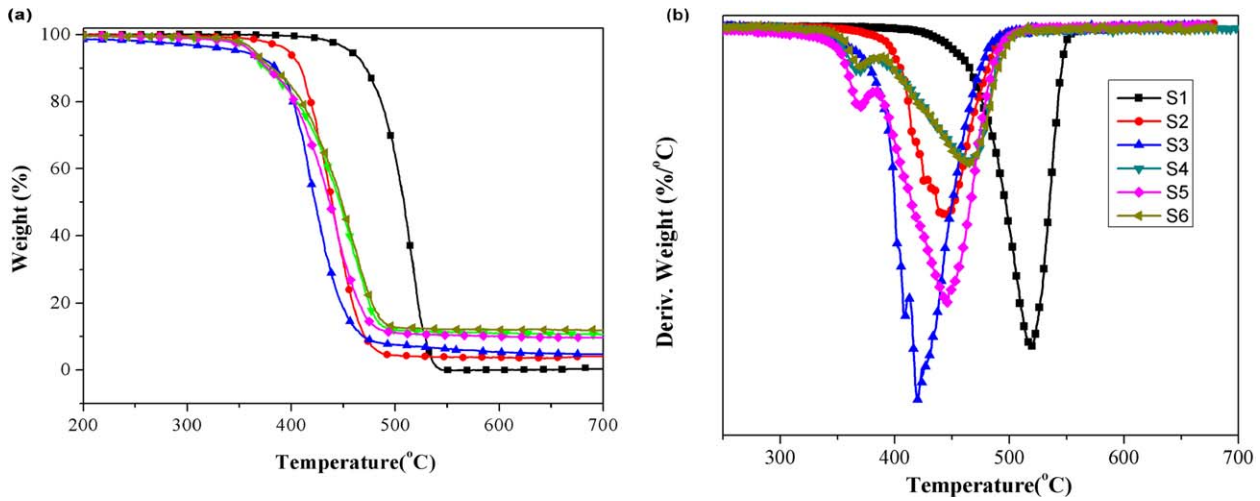

Figure 3. TGA(a) and DTG(b) curves for all formulations, measured under nitrogen atmosphere. [Color figure can be viewed in the online issue, which is available at wileyonlinelibrary.com.]

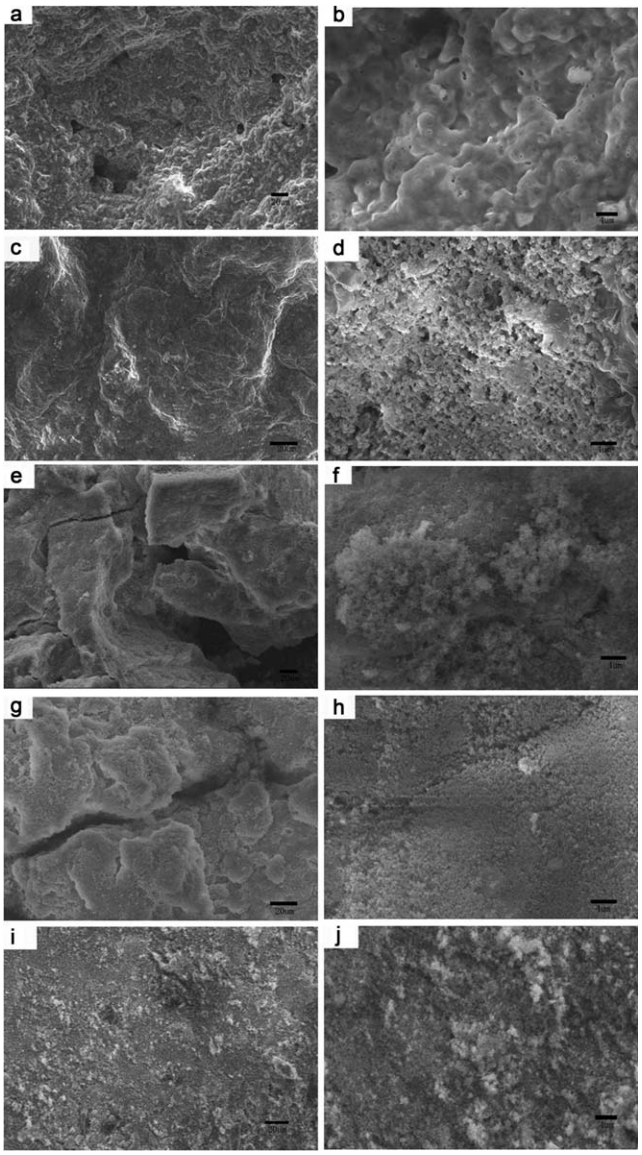

Figure 4. SEM images of residues. PA6/OP1314 (a,b), PA6/OP1314/DOPO(c,d), PA6/OP1314/SiO_2 (e,f), PA6/OP1314/DOPO+SiO_2 (2:5) (g, h), PA6/OP1314/DOPO–SiO_2 (i, j).

DOPO–SiO_2 was incorporated into PA6/OP1314, $T_{5wt\ \%}$ and the maximum mass loss rate temperature of the latter were higher than that of the former's. Furthermore, the maximum loss rate of PA6/OP1314/DOPO–SiO_2 was the lowest in all formulation, even slightly lower than the rate of PA6/OP1314/SiO_2. It could be assumed that SiO_2 can form a good protective layer to prevent from the exchange of mass and heat, thus decreasing the rate of decomposition. The residue of S6 was the highest compared with the remained residue of PA6/OP1314/SiO_2 and PA6/OP1314/DOPO, which suggested that the DOPO–SiO_2 has a synergistic effect in char formation process during the heating process. It also demonstrate that DOPO–SiO_2 had an impact on carbonization resulting in the formation of the thermally-stable char. Moreover, the TGA curve of PA6/OP1314/DOPO–SiO_2 clearly differed from PA6/OP1314/DOPO+SiO_2 which also demonstrates that SiO_2 successfully modified DOPO.

Residue Analysis

Figure 4 showed the SEM images obtained from the char residue of PA6/OP1314, PA6/OP1314/DOPO, PA6/OP1314/SiO_2, PA6/OP1314/DOPO+SiO_2, PA6/OP1314/DOPO–SiO_2. Neat PA6 had no residue after heating at 800°C for 15 minutes. The elemental analysis results are presented in Table IV. Figure 4(a,b) shows that the char residue of S2 (PA6/OP1314) had numerous differently sized holes and a rough surface structure. The heat and gas transferred through the holes, and this led to continuous burning or decomposition. Thus, it burned with melt-dripping behavior during the UL94 test. As shown in Fig. 4(c,d), the char residual of PA6/OP1314/DOPO possessed no holes on the surface of the char. However, a large number of holes with different diameters were observed in the high magnification image. PA6/OP1314/SiO_2 had compacted and dense char, which was shown in Fig. 4(e,f). However, a number of substantial flaws were found on the surface which might be a result from the poorly dispersed SiO_2. Fig. 4(g,h) showed the char of PA6/OP1314/DOPO+SiO_2 which also exhibited major flaws on the surface along with various minor flaws that can be observed in the high magnification photo. Fig. 4(i,j) presented a excellent char layer which was integrated, compact, dense and smooth. Looking more closely at the high magnification of the char residue of PA6/OP1314/DOPO–SiO_2, there were no apparent flaws due to the good dispersion of DOPO–SiO_2.

Table IV shows the contents of C, O, P, Si, and Al in the char residue of PA6/OP1314, PA6/OP1314/DOPO, PA6/OP1314/SiO_2, PA6/OP1314/DOPO+SiO_2, PA6/OP1314/DOPO–SiO_2. The weight percentage of carbon element in the char of PA6/OP1314/DOPO–SiO_2 was the higher than other formulations. The carbon content in the residue decreased with the addition of DOPO; in the char residue of PA6/OP1314, PA6/OP1314/DOPO, PA6/OP1314/SiO_2, PA6/OP1314/DOPO+SiO_2, PA6/OP1314/DOPO–SiO_2. The weight

Table IV. EDS Results of the Chars of all Formulations

		Element (wt %)				
Number	Sample	C	O	P	Si	Al
S2	PA6/OP1314	8.66	49.55	28.45	—	13.34
S3	PA6/OP1314/DOPO	7.67	52.89	29.52	—	9.92
S4	PA6/OP1314/SiO_2	8.54	51.26	9.06	23.05	8.08
S5	PA6/OP1314/DOPO + SiO_2 (2:5)	6.12	49.11	14.45	21.85	8.48
S6	PA6/OP1314/DOPO-SiO_2	11.53	54.80	10.48	18.13	5.06

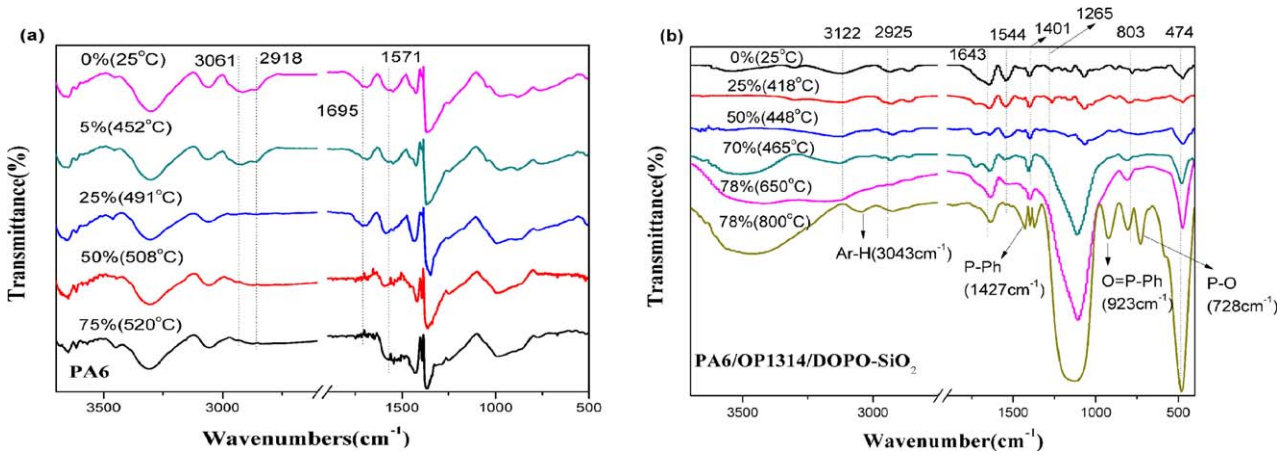

Figure 5. FTIR spectra of PA6 and PA6/OP1314/DOPO–SiO_2 after heating under different temperature consistent with the weight loss percent in TGA. [Color figure can be viewed in the online issue, which is available at wileyonlinelibrary.com.]

percentage of carbon element in the char of PA6/OP1314/DOPO–SiO_2 was the higher than other formulations. The oxygen content of S6 was higher than other formulating while the silicon content was lower than that of S5 and S4. This may have resulted from the formation of more phosphate in the char residue of PA6/OP1314/DOPO–SiO_2 after the addition of DOPO–SiO_2.

Flame-Retarding Mechanism Analysis

FTIR Analysis. It is evident that PA6/OP1314/DOPO–SiO_2 composites show a much higher flame retardancy performance than neat PA6 as outlined by the tests above. Therefore, it was necessary to demonstrate the flame-retarding mechanism.

Figure 5 shows the FTIR spectra of neat PA6 and PA6/OP1314/DOPO–SiO_2 being heated in the muffle furnace at different temperatures for 15min. No residue of pure PA6 were collected at 650 and 800°C; therefore, there are no corresponding FTIR spectra present in Figure 5(a). All of the characteristic peak intensities decreased with an increasing temperature, especially the peaks of the —CH_2— stretching vibrations (3061 and 2918 cm^{-1}), carbonyl stretching vibrations (1695 cm^{-1}), and —NH— deformation vibrations (1571 cm^{-1}) within the temperature range of 491 to 520°C. No "new" peaks were found in the spectrum of PA6 at other temperatures.

PA6/OP1314/DOPO–SiO_2 exhibited a quite different change in the FTIR spectrum with increasing temperature. As shown in Figure 5(b), the critical characteristic peak of PA6 at 800°C remained evident; which demonstrates the good thermal stability of the composites, such as the peaks of —CH2— (2936 cm^{-1}, antisymmetry stretching vibration; 2863 cm^{-1}, symmetry stretching vibration; 1397 cm^{-1}, bending vibration), and carbonyl (1643 cm^{-1}, stretching vibration). The peak of —NH— (3301 cm^{-1} antisymmetry stretching vibration; 3119 cm^{-1} stretching vibration; 1544 cm^{-1}, deformation vibration), however, tapers off and disappears at 800°C. The intensity of the existing characteristic peaks increases, such as the Si—O (1129 cm^{-1}, antisymmetric stretching vibration, 803 cm^{-1}, symmetry stretching vibration; 474 cm^{-1}, bending vibration), which resulted from the formation of SiO_2. SiO_2 can move onto the surface of the matrix to act as a physical barrier to hold back the heat and oxygen transfer during the burning process. In addition, It is interesting that the characteristic peak of P—O at 728 cm^{-1} appeared at 800°C for the formation of the phosphate salt at this high temperature. Meanwhile, R—P═O at 1265 cm^{-1} disappeared at 448°C and reappeared at 800°C (Ar—P═O(928 cm^{-1})). In correlation with the TG curve, it is speculated that a great deal of P—O and P═O groups were generated during the gaseous phase and acted as scavengers to eliminate the free radicals. Therefore, the FTIR spectrum analyzer was unable to detect the characteristic peak of P—O and R—P═O. As such, P—O or P═O reacted with the radicals and it formed into phosphate and its derivatives, whose groups can be detected by the IR detector. It should be noted that the group of P═O reappeared in the spectrum as a characteristic peak of Ar—P═O(928 cm^{-1}) which proves the effective flame retarding action of DOPO–SiO_2 in the matrix during the condensed phase. The appearance of Ar—P═O can be explained by two other points. Firstly, when the temperature increased, a number of characteristic peaks of groups with better thermal stability appeared in the spectrum which overlapped due to the low content in the matrix, such as Ar—H(3057 cm^{-1}, stretching vibration). Another reason was the new peak at 1369 cm^{-1}(P—Ph), which emerged in the FTIR spectrum at 800°C.

Py–GC/MS. The analysis of FTIR spectra at different temperatures was beneficial for explaining the flame retarding mechanism in the condensed phase. In order to investigate the flame retarding mechanism of the system during the gaseous phase, the neat PA6, PA6/OP1314 and PA6/OP1314/DOPO–SiO_2 composites were also studied with Py-GC/MS.

Figure 6 showed the pyrogram of neat PA6, PA6/OP1314 and PA6/OP1314/DOPO–SiO_2 composite after the testing of Py-GC/MS. Due to a wide variety of pyrolysis products obtained in the pyrograms which cannot clearly illustrated and analyzed the mechanism in this paper, the main pyrolysis products or representative products had been listed in Figure 6. A picture of the flame retarding mechanism is shown in Figure 7 after the analysis of Py-GC/MS. Among this, PA6 decomposed and released four products, including 5-cyano-1-pentene (C_6H_9N), caprolactam ($C_6H_{11}NO$), 2-ethylaminotetrahydrofuran ($C_3H_{13}NO$), and octanamide ($C_8H_{17}NO$). Compared to the pyrogram of neat PA6, the additives

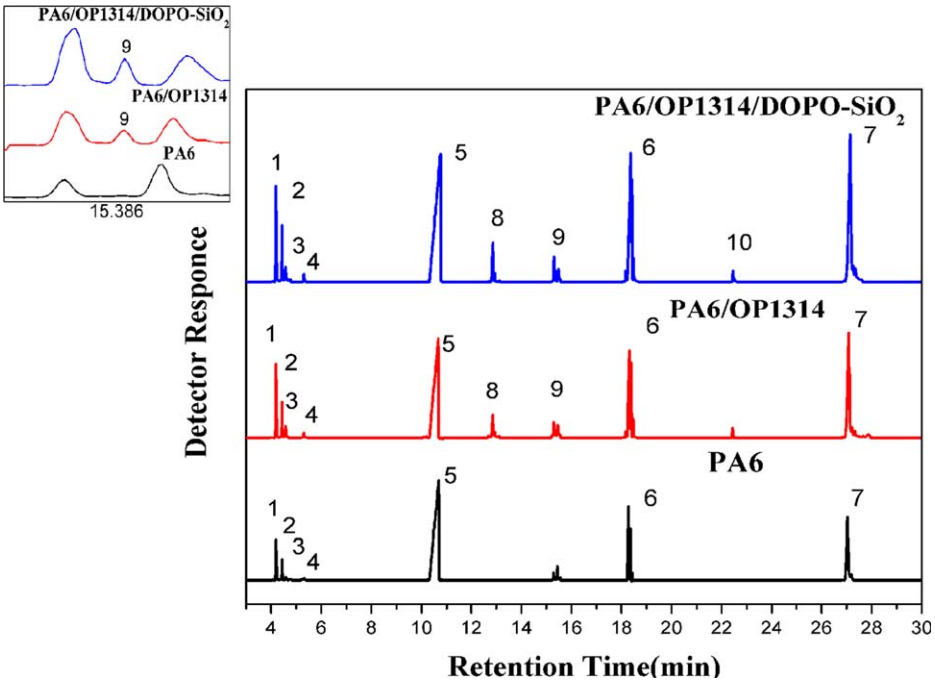

Figure 6. The program of pyrolysis products of PA6, PA6/OP1314 and PA6/ OP1314/DOPO–SiO_2. [Color figure can be viewed in the online issue, which is available at wileyonlinelibrary.com.]

of OP1314 and DOPO-SiO_2 slightly impacted the pyrolysis process of PA6, but the main pyrolysis products remained nearly the same.

Upon adding OP1314 to PA6, two new volatile products appeared, which can be seen in Figure 6. Studying closer examination into the mass spectrogram were used to analyze the compound, which cannot be accomplished by the NIST data. Firstly, the mass spectrum of the compound with a retention time of 15.386 min is shown in Figure 8(a). Because of disturbances in the free radical rearrangement reaction, a number of large mass-to-charge ratios were not taken into consideration. The m/z ratio of fragments at 41 (cyanamide) and 59 (aminoformamidine) were considered as the fragments of 126 (melamine) from the heterocyclic nitrogen ring-opening reaction. The $m/z = 81$ was regarded as the fragments of the melamine from the deamination reaction. The greatest fragment was at $m/z = 137$ which was the product of the melamine after the opening loop alkyl reacted with the radical

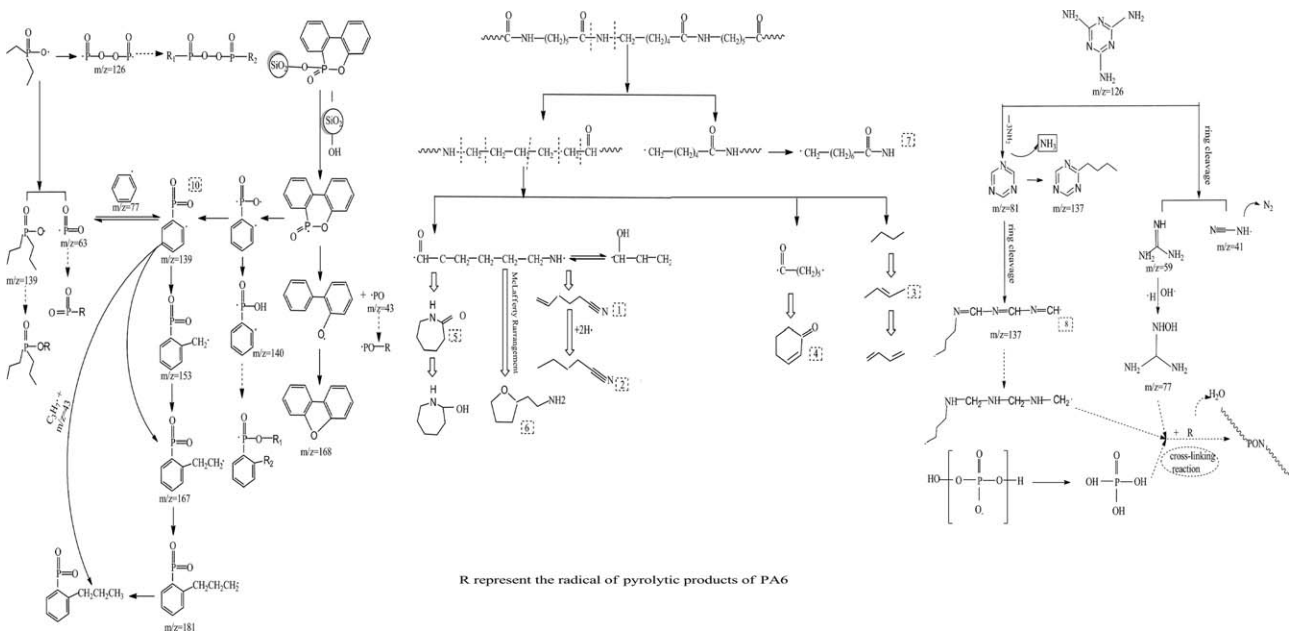

Figure 7. Schematic diagram of proposed flame-retardant mechanism model of PA6/OP1314/DOPO–SiO_2.

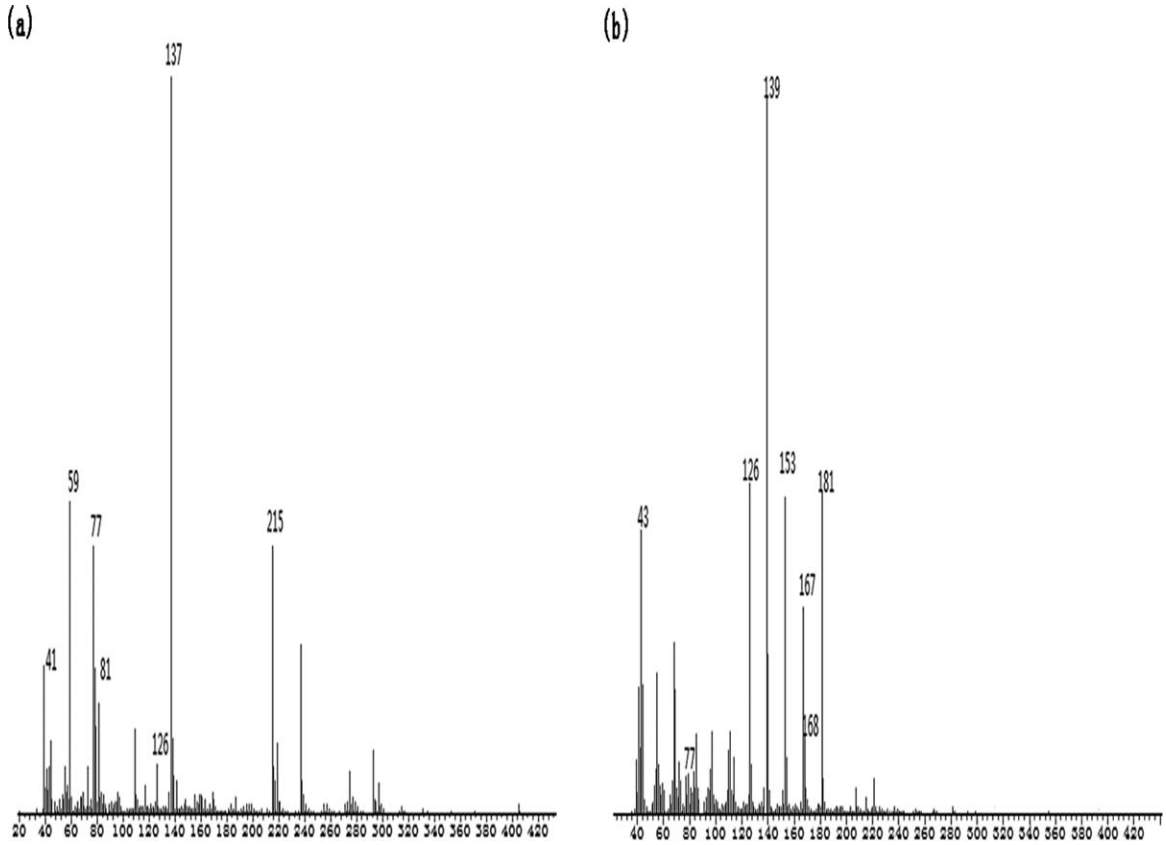

Figure 8. Mass spectra of Py products with retention times of (a) 15.386 and (b) 22.453.

from PA6. Melamine was released for the heterocyclic nitrogen ring-opening reaction when the temperature was greater than 600°C. The pyrolytic products of cyanamide can produce N_2 into the gas phase to dilute combustible gases and absorb lots of heat. The amino group and hydrogen next to the nitrogen were active, resulting in an acylation reaction, alkylation reaction, condensation and deamination. Thus the radicals with primary amine secondary amine may react with the radicals of amino groups, alkyl and carboxyl groups, which could produce water in the reaction. As such it can be speculated that the melamine has a good flame retarding effect to PA6. The pyrolysis product of 9 can potentially show phosphorus, as shown by NIST and having appeared in the program of PA6/OP1314 and PA6/OP1314/DOPO–SiO_2. However the degree to which it matched with the standard substance was so low that it cannot be entirely validated. The mass spectrogram of the product exhibited too many rearrangement fragments to analyze them accurately. Therefore, a number of assumptions on hypophosphite and phosphate are summarized in Fig 7, reflected in various other forms of research.[18,21,22] Hypophosphite produced PO· and PO_2· radicals to catch radicals in the gas phase. Phosphate reacted with the Py products of PA6 and melamine to form a crosslinked structure.

By loading DOPO-SiO_2, the pyrogram showed a new product (retention time = 22.453 min) which was illustrated in the mass spectrogram [Fig. 8(b)]. The main fragment was considered to be the Ph–PO_2 radical. After closer consideration of the mass spectrogram, Ph–PO_2 was shown to react as a radical scavenger and form stable phenyl-containing products. This was further confirmed by the results from FTIR, working as a radical scavenger above 448°C in the gaseous phase and producing compounds with PO_2 and phenyl group in the condensed phase. This latter fact was then detected by the IR detector. It was certainly of note that the double phosphate radicals ($m/z = 126$) which were found in the mass spectrogram, were able to form a more stable product.

Combining the FTIR analysis with pyrolysis GC/MS at various temperatures, it can be concluded that OP1314 and DOPO–SiO_2 exhibit flame retarding effects on PA6 in the gaseous phase and condensed phase. Further PO·, PO_2· and P_2O_4· can act as free radical scavengers to eliminate the combustible gases and melamine can react with the pyrolytic products from the PA6 to enhance the thermal stability.

Viscoelastic Properties

The viscoelastic characteristics were used as an assistant test for flammability.[19] In order to further explore the flame retarding mechanism in terms of the mutual effects between matrix and additives, the rheological properties of neat PA6, PA6/OP1314, PA6/OP1314/DOPO+SiO_2, PA6/OP1314/DOPO–SiO_2 were analyzed. Fig. 9(a) and Fig. 9(b) showed the storage modulus (G′) and the loss modulus (G″) as a function of frequency. Compared with neat PA6, the G′ and G″ of the composites increased at varying amplitudes. The increasing amplitude for the G′ of PA6/OP1314 and PA6/OP1314/DOPO–SiO_2 is higher than that of G″,

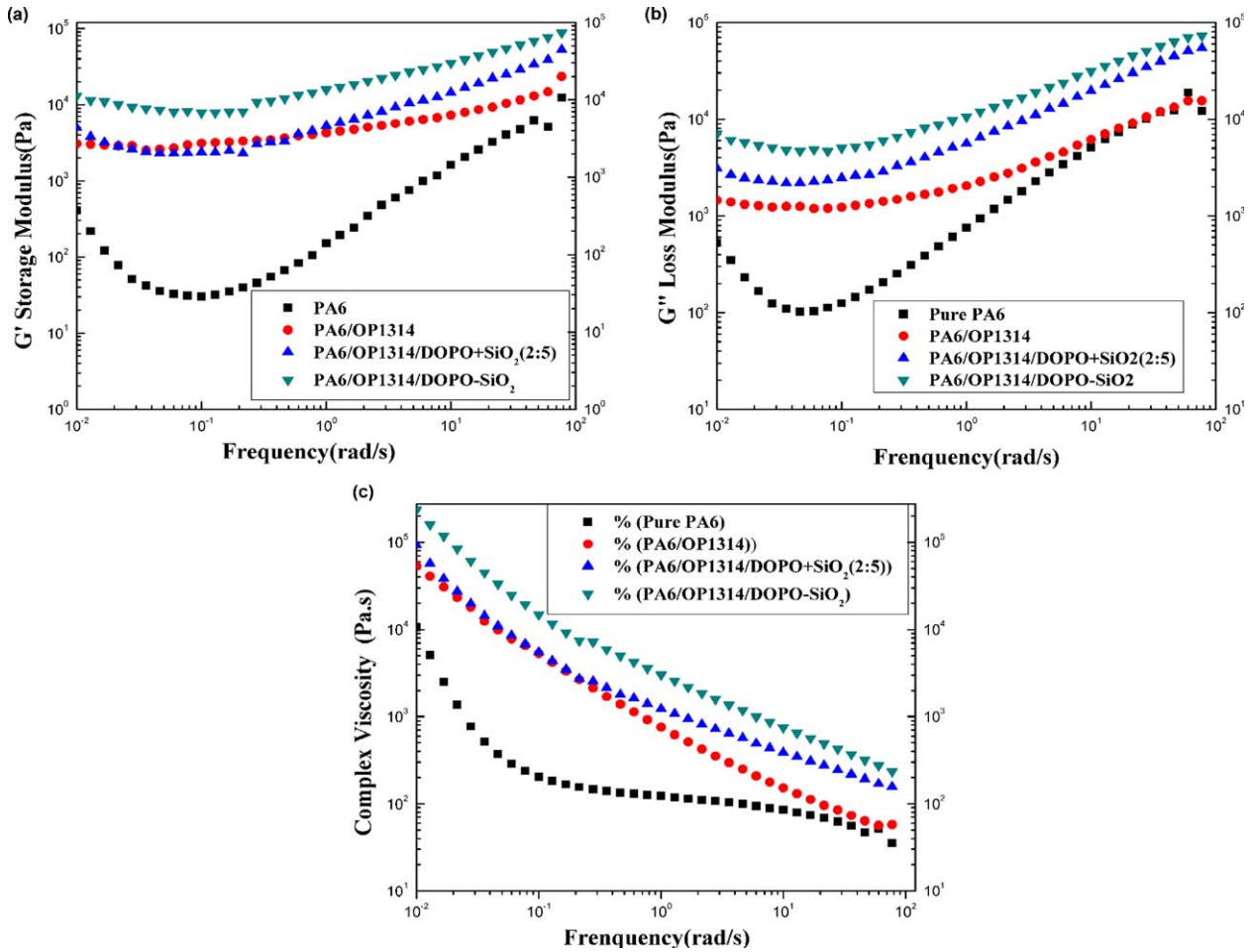

Figure 9. The viscoelastic characteristic of PA6, PA6/OP1314, PA6/OP1314/DOPO+SiO_2 (2:5) and PA6/OP1314/DOPO–SiO_2: the relationship of storage modulus (a), loss modulus (b), complex viscosity (c) with a strain of 1% from 0.01 to 100 rad/s at the temperature of 230°C. [Color figure can be viewed in the online issue, which is available at wileyonlinelibrary.com.]

while the PA6/OP1314/DOPO+SiO_2 exhibits opposing results. It can be assumed that the PA6/OP1314 composite is highly compatible with the addition of OP1314, while the addition of DOPO and SiO_2 is harmful to the compatibility of the composites. It is interesting that the PA6/OP1314/DOPO–SiO_2 composites became better than PA6/OP1314 composites, which can be proved by analyzing Fig. 9(c). The complex viscosity of PA6/OP1314/DOPO–SiO_2 was the highest, which is relevant for the high compatibility and dispersibility. The higher compatibility induces stronger intermolecular forces and a higher elastic modulus. Well-dispersed particles in the matrix are also beneficial for improving the viscosity. Thus, it has been demonstrated that DOPO–SiO_2 exhibits its high compatibility and dispersibility in the matrix. The increase in complex viscosity also controls the dripping phenomenon, which explains the dripping results from of UL 94 when SiO_2 and DOPO–SiO_2 were added to the PA6 matrix.

CONCLUSIONS

In this paper, the modification of DOPO on the surface of a SiO_2 nanoparticle was successfully achieved within a one-step process. PA6 composites with an excellent flame retardancy performance were introduced as a combination of a P–N flame retardant and DOPO–SiO_2. Furthermore, the FR mechanism of PA6/OP1314/DOPO–SiO_2 were able to be explained through the effects in the gaseous and condensed phase. In the gaseous phase, hypophosphite produced PO·, PO_2· and P_2O_4· radicals to capture active radicals. DOPO–SiO_2 turned into PO_2· with phenyl or PO_2· and PO· radicals acted as a radical trap, while melamine released N_2, NH_3 and H_2O to dilute the volatile gases. In the condensed phase, the phosphate and melamine reacted with the degradation products of PA6 to form cross-linked structures, while the generated SiO_2 acted as a physical barrier on the surface of the matrix to insulate the transfer of heat and oxygen.

ACKNOWLEDGMENTS

Financial support from East China University of Science and Technology is gratefully acknowledged.

REFERENCES

1. Zhong, Y. H.; Wu, W.; Wu, R.; Luo, Q. L.; Wang, Z. *Polym. Degrad. Stab.* **2014**, *105*, 166.
2. Bourbigot, S.; Samyn, F.; Turf, T.; Duquesne, S. *Polym. Degrad. Stab.* **2010**, *95*, 320.

3. Liu, Y. L.; Tsai, S. H. *Polymer* **2002**, *43*, 5757.
4. Buczko, A.; Stelzig, T.; Bommer, L.; Rentsch, D.; Heneczkowski, M.; Gaan, S. *Polym. Degrad. Stab.* **2014**, *107*, 158.
5. Chen, X. X.; Gu, A. J.; Liang, G. Z.; Yuan, L.; Zhuo, D. X.; Hu, J. T. *Polym. Degrad. Stab.* **2012**, *97*, 698.
6. Qian, X. D.; Pan, H. F.; Xing, W. Y.; Song, L.; Yuen, R. K. K.; Hu, Y. *Ind. Eng. Chem. Res.* **2012**, *51*, 85.
7. Konig, A.; Kroke, E. *Fire Mater.* **2012**, *36*, 1.
8. Konig, A.; Kroke, E. *Polym. Adv. Technol.* **2011**, *22*, 5.
9. Schafer, A.; Seibold, S.; Lohstroh, W.; Walter, O.; Doring, M. *J. Appl. Polym. Sci.* **2007**, *105*, 685.
10. Yang, S.; Wang, J.; Huo, S. Q.; Cheng, L. F.; Wang, M. *Polym. Degrad. Stab.* **2015**, *115*, 63.
11. Qian, L. J.; Ye, L. J.; Qiu, Y.; Qu, S. R. *Polymer* **2011**, *52*, 5486.
12. Wang, X.; Hu, Y.; Song, L.; Xing, W. Y.; Lu, H. D. A.; Lv, P.; Jie, G. *Polymer* **2010**, *51*, 2435.
13. Gu, H. W.; Guo, Y. B.; Wong, S. Y.; He, C. B.; Li, X.; Shim, V. P. W. *Compos. Sci. Technol.* **2013**, *75*, 62.
14. Gendre, L.; Njuguna, J.; Abhyankar, H.; Ermini, V. *Mater. Des.* **2015**, *66*, 486.
15. Gong, J.; Niu, R.; Tian, N.; Chen, X.; Wen, X.; Liu, J.; Sun, Z.; Mijowska, E.; Tang, T. *Polymer* **2014**, *55*, 2998.
16. Wu, Z. H.; Qu, J. P.; Zhao, Y. Q.; Tang, H. L.; Wen, J. S. *J. Thermoplast. Compos.* **2015**, *28*, 981.
17. Zhao, B.; Chen, L.; Long, J. W.; Chen, H. B.; Wang, Y. Z. *Ind. Eng. Chem. Res.* **2013**, *52*, 2875.
18. Kashiwagi, T.; Mu, M. F.; Winey, K.; Cipriano, B.; Raghavan, S. R.; Pack, S.; Rafailovich, M.; Yang, Y.; Grulke, E.; Shields, J.; Harris, R.; Douglas, J. *Polymer* **2008**, *49*, 4358.
19. Hu, Z.; Chen, L.; Lin, G. P.; Luo, Y.; Wang, Y. Z. *Polym. Degrad. Stab.* **2011**, *96*, 1538.
20. Zhao, B.; Hu, Z.; Chen, L.; Liu, Y.; Liu, Y.; Wang, Y. Z. J. *Appl. Polym. Sci.* **2011**, *119*, 2379.
21. Ebdon, J. R.; Price, D.; Hunt, B. J.; Joseph, P.; Gao, F. G.; Milnes, G. J.; Cunliffe, L. K. *Polym. Degrad. Stab.* **2000**, *69*, 267.
22. Ebdon, J. R.; Hunt, B. J.; Joseph, P.; Konkel, C. S.; Price, D.; Pyrah, K.; Hull, T. R.; John Milnes, G.; Hill, S. G.; Lindsay, C. I.; McCluskey, J.; Robinson, I. *Polym. Degrad. Stab.* **2000**, *70*, 425.